Turk J Phy
25 (2001) , 195 – 213.
© TÜBİTAK

Viscous Dissipation of Magnetosonic Waves in Solar Corona

Belinda KALOMENI, D. Özlem HÜRKAL,
E. Rennan PEKÜNLÜ, Kadri YAKUT
University of Ege Dept. of Astronomy and Space Sciences,
Bornova 35100 Izmir-TURKEY

Received 31.05.2000

Abstract

Wave propagation and dissipation of magnetosonic waves are considered in an inhomogenous viscous coronal plasma permeated by a spatially varying magnetic field. In the linear magnetohydrodynamic approximation the dispersion relation yields two wave modes, fast and slow respectively. Depending on the physical parameters of the medium the damping length scales of the modes show varying behaviours. Damping length scales of the modes show sudden decrease at relevant heights. These drops may be due to phase mixing and resonance absorption. Wave flux density of the magnetosonic waves turns out to be of the order of 10^6 erg cm^{-2} s^{-1}. This is high enough to replace the lost energy through optically thin emission and the thermal conduction down to the transition region

Key Words: magnetosonic waves, solar corona, dispersion relation, damping length scale.

1. Introduction

One of the long-standing problems of solar atmosphere is its 'anomalous' temperature profile. As is well-known that the temperature of the solar photosphere is 5780 K. If one moves radially out then one reaches at the *temperature minimum* occurring at about 500 km above the photosphere. Then the temperature rises again all through the chromosphere but slowly. The sharpest gradient of the temperature profile is throughout the transition region. In the corona, the temperature keeps rising but comparatively less sharply, reaching $1 - 5 \times 10^6$ K at the upper corona [1].

Such a hot plasma is bound to lose energy through optically thin radiation and thermal conduction to the transition region below. These losses must be balanced by a heat source

to maintain the coronal temperatures. The long-sought-for answer to the question, "By what mechanism or mechanisms is the corona being heated ?" has yet to be satisfactorily given.

Although it will not be addressed directly in this study, a related problem to the one posed above is the existence of high speed solar wind. Observations of high speed solar wind indicate the need for a substantial energy flux that is transported outward from the coronal base by some process other than convection or classical thermal conduction. Undamped Alfvén waves are claimed to be capable of supplying the necessary energy flux [2][3][4][5][6][7].

It is obvious that all the carriers of mechanical energy derive their energy from the nuclear processes in the solar core. This energy is then transported to the solar surface in the form of radiation and convection. Mechanical energy is generated in the surface convection zone. Since the density near the top boundary of this zone is smaller the plasma motions become larger there and waves are quite easily generated in a narrow surface layer.

Plasma motions in the convection zone can be described by a common temporal and spatial turbulence spectrum. This spectrum consists of a distribution of plasma bubbles of all sizes and lifetimes.

Energy is transported by macroscopic mechanisms (transport with velocity v and work due to the pressure) and by microscopic mechanisms (thermal conductivity, viscosity, resistivity, Hall effect, etc.). The microscopic mechanisms and the corresponding terms in the energy and heat equations are called *dissipative*. These mechanisms increase the entropy of the plasma and result in the conversion of mechanical energy into heat [8]. In dissipative processes organized motions of waves or potential energy is converted into random thermal motions [9].

2. The Relative Importance of Processes for Dissipation

In this subsection we'll examine the relative importance of four dissipative processes: viscosity, thermal conduction, resistivity and Hall effect. For this purpose, we define dimensionless parameters, so-called 'numbers' by referring to the induction equation, the equation of motion and the energy equation. The equation giving the temporal and the spatial evolution of the magnetic field is called the induction equation :

$$\frac{\partial \mathbf{B}}{\partial t} = \nabla \times (\mathbf{v} \times \mathbf{B}) + \eta \nabla^2 \mathbf{B}, \tag{1}$$

where $\mathbf{v}$ is the average velocity of the plasma in its bulk motion; $\eta = (\mu\sigma)^{-1}$ is the magnetic diffusivity; μ is the magnetic permeability; σ^{-1} is the electrical resistivity. The first term on the right hand side of the induction equation is called the convective term and the second term is called the diffusive term.

The *Magnetic Reynolds number,* $R_m = l_0 V_0/\eta$, is the ratio of the convective term to the diffusive term, where V_0 is typical plasma speed and l_0 is the length scale; it is a measure of the strength of the coupling between the flow and the magnetic field[10]. In

the solar atmosphere $R_m \gg 1$ so that the coupling is strong, i.e., plasma is "frozen into" the magnetic field. That is to say, plasma and the magnetic field have no relative velocity with respect to each other.

On the other hand, the motion of the plasma blob under various forces is described by the equation of motion:

$$\rho\frac{\partial \mathbf{v}}{\partial t} + \rho(\mathbf{v}\cdot\nabla)\mathbf{v} = -\nabla p + (\nabla\times\mathbf{B})\times\mathbf{B}/\mu + \rho v\left[\frac{4}{3}\nabla(\nabla\cdot\mathbf{v}) - \nabla\times\nabla\times\mathbf{v}\right] \qquad (2)$$

where ρ is the mass density; p is the pressure; and ρv is the viscosity coefficient. If we take the ratio of the inertial term (left hand side term) to the viscous term then we get the Reynolds number, $Re = l_0 V_0/v$. The *Magnetic Prandtl Number* is defined as $P_m = R_m/Re = v/\eta$. The Prandtl Number $Pr = v/\kappa$, is a measure of the ratio of viscous to thermal diffusion.

The relative importance of viscosity and resistivity is characterized by the magnetic Prandtl number P_m. If we substitute into $P_m = v/\eta$ the parameter values for an active region of the solar corona, we get, $P_m \sim 10^{10}$. This estimate shows that dissipation due to resistivity can be neglected in comparison with dissipation due to viscosity.

Now let us see the relative importance of viscosity and Hall effect. This is characterized by the dimensionless parameter $\tau_e\omega_{ce}P_m^{-1}$ which is of the order of 10^{-3} in an active region. t_e and ω_{ce} are electron collision time and electron cyclotron frequency, respectively. The above given value (10^{-3}) implies that we can neglect the Hall effect in comparison with the effect of viscosity [11].

The relative importance of viscosity and thermal conductivity is characterized by the $\beta^{-1}Pr$ where $\beta = n_e T_e/(B^2/2\mu_0)$ another dimensionless parameter which measures the relative importance of plasma pressure and magnetic pressure [12]. In an active coronal region where we shall deal with the wave propagation and dissipation, $\beta \sim 0.016$. In this case, the relative importance of viscosity and thermal conductivity is $\beta^{-1}Pr \sim 1$ which means that viscosity and thermal conductivity are of the same importance. Nevertheless, the inclusion of thermal conductivity makes the dispersion relation analytically intractable. Therefore, the solution of the dispersion relation with its most general form will be put off for future study.

3. Observational Evidence for the Existence of MHD Waves in the Solar Corona

In the previous section we demonstrated that two dissipative processes out of four are qualified for the coronal heating. But are we sure that MHD waves can propagate through the corona? Are there any observational evidence as to their existence in the solar atmosphere?

Optically thin emission lines of coronal plasma can provide information concerning the velocity fluctuations associated with MHD waves (see [13][7]). To isolate line broadening due to MHD waves, it is necessary to observe line widths of high temperature coronal lines (formation temperature $> 10^6 K$) above the limb ($> 1.10 R_\odot$) where broadening of

this nature becomes dominant. Early evidence for broadening of transition region (TR) emission lines has been supplied by *Skylab* [14][15][16] and by *OSO* 8 observations [17][18]. However, *Skylab* and *OSO* 8 observations are restricted to moderate temperature lines formed in the TR (i.e., C IV , N IV , O V with temperatures of formation $< 5 \times 10^5 K$) and in regions very near the limb ($< 20''$ above the limb), line broadening due to MHD waves cannot be distinguished from other broadening mechanisms in the above mentioned observations.

Through the 1990s, convincing evidence for the existence of MHD waves in the solar atmosphere has been accumulated. For instance, Hassler et al [7] using a Colorado University's sounding rocket experiment data provided high resolution EUV spectra along a solar diameter and out to $1.2R_\odot$ with spatial resoultion of $20'' \times 60''$. Spectra contained TR and coronal emission lines, i.e., Mg X $\lambda\lambda$ 609 & 625, Fe XII λ 1242, O V λ 629, N V $\lambda\lambda$ 1238 & 1242. All six lines displayed line broadening above the limb. As is well-known, there are a series of effects such as opacity, systematic flows, spatial variation of thermal Doppler width and MHD waves causing line broadening. Hassler et al. [7] seem to have performed preliminary calculations on these effects so to conclude that the most likely cause is the presence of MHD waves in the corona.

A similar study was carried out by Saba & Strong [6] with *Solar Maximum Mission (SMM)* data. *Flat Cyrstal Spectrometer (FCS)* on board SMM took spectra of six coronal X-ray line near a quiescent active region (QAR) loop. These lines are produced by the transitions $1s - 2p^2 P_{1/2,3/2}$ of the H-like O VIII ion and the $1s^2 - 1s2p$ transition of the He-like ions Ne IX , Mg XI , Si XIII , S XV and Fe XXV. Ratios of the line fluxes for various pairs of four ions (O VIII , Ne IX , Mg XI , Si XIII) were compared with the ratios of their emissivity functions to determine $\overline{T}_e$, the average electron temperature, which was found to be $\overline{T}_e = 3.0 \pm 0.1 \times 10^6 K$. If the measured line widths were to be attributed to thermal Doppler motions exclusively, a significant amount of plasma with $\overline{T}_e \geq 6 \times 10^6 K$ would be required. Such high temperature plasma, authors claimed, would be detected by high energy FCS and BCS (Brent Cyrstal Spectrometer) channels. If the temperature equivalent of the measured line widths were as high as $6 \times 10^6 K$ then spectrometers would detect flux in Si XIII channel 100 times more than actually observed [6]. The absence of this flux indicates that the excess width is brought about by non-thermal processes, either by MHD waves or non-thermal motions along the line of sight.

An optically thin line profile assuming a Gaussian distribution gives a full width at half maximum as below [19]:

$$FWHM^2 = 4 \ln 2 \left(\frac{\lambda}{c}\right)^2 \left(\frac{2kT_i}{M} + \frac{1}{2}\langle \delta v^2 \rangle^2\right), \tag{3}$$

where λ is the wavelength; c is the speed of light; k_B is Boltzmann constant; T_i is the ion temperature; M is the ion mass; and $< \delta v^2 >$ is the rms velocity of the perturbation that causes the non-thermal broadening of the line. Saba & Strong [6] claim that if the broadening is due to the motions perpendicular to the magnetic field caused by Alfvén

waves, then the energy flux carried by these waves is sufficient to replace the thermal flux lost through optically thin radiation and thermal conduction to the TR below, i.e., $F_{Alf} = \rho\langle\delta v^2\rangle V_A \approx 3.1 \times 10^5$ erg cm$^{-2}s^{-1} \approx F_{th}$.

Later, Doyle et al [4] combined SUMER, LASCO & UVCS data and Banerjee et al [5] using SUMER data of SOHO evaluated the line width of Si VIII in the polar coronal holes. Line width of Si VIII was found to be continuously increasing above the solar limb. Simultaneous measurements of electron density showed that, $\langle\delta v^2\rangle^{1/2} \propto \rho^{-1/4}$. This observational fact supports the theoretical prediction that the rms velocity of undamped Alfvén waves is inversely proportional to the quadratic root of the density. Using the measured electron density and the rms velocity one can calculate the Alfvén wave's flux density (see Banerjee et al [5]). From their data set at $120''$ above the limb for the North Polar Coronal Hole, using $N_e = 4.8 \times 10^7$ cm^{-3}, $\langle\delta v^2\rangle = 2 \times (43.9$ km $s^{-1})^2$ they find $F_{Alf} = 4.9 \times 10^5$ erg cm $^{-2}s^{-1}$ for $B = 5$ gauss which is only slightly lower than the requirements for a coronal hole with a high speed solar wind flow.

In short Doyle et al [4] claim that the Alfvén waves with an amplitude of 30 - 50 km s^{-1} (as observed) at the base of the coronal hole can generate non-linear solitary type of waves which can contribute significantly to solar wind acceleration in open magnetic field structures.

4. MHD Waves in Quiescent Active Regions

In the previous chapter, we have seen the observational evidence for the existence of MHD waves in the solar corona. In this chapter we shall deal with magnetosonic wave propagation and dissipation in the compressible, viscous coronal plasma.

In the past, Ruderman [20] investigated viscous damping of surface waves at a magnetic interface. He did not take thermal conduction into account and to solve his dispersion relation he assumed the small damping approximation. But the crux of the matter lies in the fact that when MHD equations are to be solved self-consistently one should not make assumptions a priori to their dissipational character; it should rather emerge quite naturally from the solution. Van der Linden & Goosens [21] incorporated thermal conduction into their equations but do not take viscosity in search of thermal instabilities in a slab model. Cargill & Hood [22] also incorporate thermal conduction in their investigation but do not include viscosity. Porter et al [23] [24] take both viscosity and thermal conductivity into account but in the first paper [23] they assumed an homogeneous plasma and a uniform magnetic field ; in the second paper [24] they assumed an inhomogeneous plasma but preserved magnetic field uniformity.

The major difference between past investigations and the present investigation lies in the fact that the present one includes inhomogeneity, both in plasma disribution and magnetic field. In our investigation, plasma density ρ and plasma pressure p are assumed to be a function of height (z) from the coronal base:

$$\rho(z) = \rho_0 \exp(-z/\Lambda_p) \; ; \quad p(z) = p_0 \exp(-z/\Lambda_p) \tag{4}$$

where, $\rho_0 = \overline{\mu} m_p n = 0.6 \times 1.6 \times 10^{-27} \times 3 \times 10^{15} = 2.8 \times 10^{-12}$ kgm^{-3} is the mass density

at the coronal base; $\overline{\mu}$ is the mean atomic weight; m_p is the proton mass; n is the number density; Λ_p is the pressure scale height and is given as

$$\Lambda_p = 50T(r/r_\odot)^2 m = 50 \times 2 \times 10^6((6.96 \times 10^8 + z)/6.96 \times 10^8)^2 m, \tag{5}$$

where T is temperature; $r_\odot$ is the solar radius; and r is the distance from the Sun's center.

The plasma, the properties of which are described above, is permeated by dipole - like magnetic field and is given as,

$$B(z) = B_0 \exp(-z/\Lambda_B), \tag{6}$$

where Λ_B is magnetic field scale height and its value is taken as 2×10^8 m [10]; and B_0 is the value of magnetic field at the coronal base and is given as 0.005 T [11]. Alfven velocity can be expressed in terms of length scales and z as

$$V_A(z) = V_{A0} \exp(-\frac{2-\delta}{2\Lambda_B} z), \tag{7}$$

where $V_{A0} = 2.5 \times 10^6 ms^{-1}$ is the velocity at the coronal base and δ is the ratio of the scale heigths: $\delta = \Lambda_B/\Lambda_p$ [25].

Now, we can investigate the wave propagation and dissipation characteristics of magnetosonic waves in coronal plasma which is assumed to be viscous dissipative. This investigation will be carried out in the linearized MHD context.

5. The Basic MHD Equations

The basic equations for the investigation of wave propagation and dissipation in a plasma are the continuity of mass, momentum and energy, together with the induction equation, in the form,

$$\frac{\partial \rho}{\partial t} + \mathbf{v} \cdot \nabla \rho + \rho \nabla \cdot \mathbf{v} = 0 \tag{8}$$

$$\rho \frac{\partial \mathbf{v}}{\partial t} + \rho(\mathbf{v} \cdot \nabla)\mathbf{v} = -\nabla p + (\nabla \times \mathbf{B}) \times \mathbf{B}/\mu + \rho v \left[\frac{4}{3}\nabla(\nabla \cdot \mathbf{v}) - \nabla \times \nabla \times \mathbf{v}\right] \tag{9}$$

$$\frac{Dp}{Dt} - \frac{\gamma p}{\rho}\frac{D\rho}{Dt} = 0 \tag{10}$$

$$\frac{\partial \mathbf{B}}{\partial t} = \nabla \times (\mathbf{v} \times \mathbf{B}) \tag{11}$$

$$\nabla \cdot \mathbf{B} = 0, \tag{12}$$

where $\gamma = 5/3$ is the adiabatic index.

Since we are after plane wave solutions we assume that all the variables hydrodynamic and electromagnetic alike, change as, $\exp[i\mathbf{k} \cdot \mathbf{r} - \omega t)]$, i.e., $\mathbf{v_1}(\mathbf{r}, t) = \mathbf{v_1} \exp[i(\mathbf{k} \cdot \mathbf{r} - \omega t])$;

where $\mathbf{v_1}$ is the rms velocity inferred from observations and given above as $\langle \delta v^2 \rangle$; $\mathbf{k}$ is the wave vector; ω is the wave frequency; t is the time; $\mathbf{r}$ is the distance from the source.

In linear approximation wherein perturbation quantities are assumed to be small compared to equilibrium values therefore have $P_1 \ll P_0; B_1 \ll B_0; \rho_1 \ll \rho_0; v_1 = \langle \delta v^2 \rangle$. Now, $P = P_0 + P_1; B = B_0 + B_1; \rho = \rho_0 + \rho_1$ and v_1 are all substituted into equations (8) - (12) and the result is:

$$\frac{\partial \rho_1}{\partial t} + \mathbf{v_1} \cdot \nabla \rho_0 + \rho_0 \nabla \cdot \mathbf{v_1} = 0 \tag{13}$$

$$\rho_0 \frac{\partial \mathbf{v_1}}{\partial t} + \rho_0 (\mathbf{v_1} \cdot \nabla) \mathbf{v_1} = -\nabla p_1 + (\nabla \times \mathbf{B_1}) \times \mathbf{B}_0 / \mu + \rho v \left[\frac{4}{3} \nabla (\nabla \cdot \mathbf{v_1}) - \nabla \times \nabla \times \mathbf{v_1} \right] \tag{14}$$

$$\frac{\partial p_1}{\partial t} + (\mathbf{v}_1 \cdot \nabla) p_0 - c_s^2 \left[\frac{\partial \rho_1}{\partial t} + (\mathbf{v}_1 \cdot \nabla) \rho_0 \right] = 0 \tag{15}$$

$$\frac{\partial \mathbf{B}_1}{\partial t} = \nabla \times (\mathbf{v}_1 \times \mathbf{B}_0) \tag{16}$$

$$\nabla \cdot \mathbf{B}_1 = 0. \tag{17}$$

Equation set (13)-(17) may be reduced to a single equation by differentiating Equation (14) with respect to time and substituting for $\partial \rho_1 / \partial t; \partial p_1 / \partial t$ and $\partial B_1 / \partial t$ from Equations (13), (15)and (16), respectively. The temporal and the spatial operators are also replaced by the below equivalents [26]:

$$\frac{\partial}{\partial t} \to -i\omega \quad ; \quad \nabla \to ik. \tag{18}$$

The condition that must be satisfied in order for the system of Equations (13) - (17) to yield a non-trivial solution gives a relation between ω and $\mathbf{k}$ called the *dispersion relation*. This condition leads us to the dispersion relation of the fourth order in $\mathbf{k}$:

$$\left[c_s^2 \alpha i\omega - \frac{4}{3}\alpha^2\omega^2 - \frac{4}{3}\alpha i\omega V_A^2 - c_s^2 V_A^2 \right] k^4 + \left[-\frac{7}{3}\alpha i\omega^3 + V_A^2\omega^2 - c_s^2\omega^2 \right] k^2 + \omega^4 = 0, \tag{19}$$

where $i = \sqrt{-1}$; and $\alpha = v\rho/\rho_0$.

It means that we have two separable quadratic equations in $\mathbf{k}$. Each equation represents one wave mode. These modes are called as "fast" and "slow" with respect to their phase velocities. Equation (19) is reduced to a quadratic equation by the substitution $k^2 = K$.

$$\left[c_s^2 \alpha i\omega - \frac{4}{3}\alpha^2\omega^2 - \frac{4}{3}\alpha i\omega V_A^2 - c_s^2 V_A^2 \right] K^2 + \left[-\frac{7}{3}\alpha i\omega^3 + V_A^2\omega^2 - c_s^2\omega^2 \right] K + \omega^4 = 0 \tag{20}$$

For the sake of simplicity in the solution of Equation (20), we'll use abbrevations for the coefficients, i.e., $A = c_s^2\alpha i\omega - \frac{4}{3}\alpha^2\omega^2 - \frac{4}{3}\alpha i\omega V_A^2 - c_s^2 V_A^2$ and $B = -\frac{7}{3}\alpha i\omega^3 + V_A^2\omega^2 - c_s^2\omega^2$.

With these substitutions Equation (20) becomes

$$AK^2 + BK + \omega^4 = 0. \tag{21}$$

The solution of Equation (21) is given as

$$K_{1,2} = \frac{-B \mp \sqrt{B^2 - 4AC}}{2A}. \tag{22}$$

Since the expression under the radical is complex, the solution is sought by De Moivre formula :

$$\sqrt[n]{z} = \sqrt[n]{r}\left[\cos\left(\frac{\theta}{n} + \frac{2m\pi}{n}\right) + i\sin\left[\frac{\theta}{n} + \frac{2m\pi}{n}\right]\right], m = 0, 1, 2, \ldots (n-1), \tag{23}$$

where $z = x + iy = r(\cos\theta + i\sin\theta)$.

In our case, $x = -\frac{1}{9}\alpha^2\omega^6 + (c_s^2\omega^2 + V_A^2\omega^2)^2$ and $y = i\left(\frac{2}{3}\alpha\omega^5 c_s^2 + \frac{2}{3}\alpha V_A^2\alpha^5\right)$ and $r = \sqrt{x^2 + y^2}$. In Equation (22) the plus sign before the radical refers to the fast mode and minus sign to the slow mode. There are two roots for the square root of a complex number. Therefore the solution of the equation (23) yields four Ks and only those with positive imaginary parts are the candidates to transfer energy to the medium, that is to say, the positive imaginary part ensures wave damping.

The solution of Equation (23) finally becomes:

$$k_{\mp}^2 = \frac{-c_s^2\omega^2 + V_A^2\omega^2 - \frac{7}{3}\alpha i\omega^3 \mp \sqrt{r}\left[\left(\frac{1}{2} + \frac{x}{2r}\right)^{\frac{1}{2}} + i\left(\frac{1}{2} - \frac{x}{2r}\right)^{\frac{1}{2}}\right]}{\left(\frac{8}{3}\alpha^2\omega^2 + 2c_s^2 V_A^2\right) + i\left(\frac{8}{3}\alpha V_A^2\omega - 2c_s^2\alpha\omega\right)}, \tag{24}$$

where, as we already stated above, the plus sign before the radical refers to the fast mode and minus sign to the slow mode.

It is clearly seen from Equation (24) that the wave vector is complex, i.e., $k = k_r + ik_i$. The damping length scale, by definition, is the inverse of k_i, $1/k_i$.

In our calculations we have used three free parameters, i.e., temperature (T), magnetic field length scale (Λ_B) and period (P). Since magnetic field measurements based on Zeeman splitting in the corona are extremely difficult, due to non-thermal broadening of the lines, one is bound to make assumptions on $\Lambda_B \cdot \Lambda_B$ assumes three different values, i.e., 10 7, 10 8, 10 9 m [10]. On the other hand, temperature measurements are more reliable than that of Λ_B. Nevertheless, we have adopted two values for temperature: $T = 1.3 \times 10^6 K$ [7] and $T = 3 \times 10^6 K$ [6]. The results of periodic intensity fluctuations indicate that MHD waves with periods 141 s, 235 s, 312 s [27] are present in the corona. Therefore, on the basis of the above observational measurements we have assumed the presence of waves with periods of 100 s, 200 s, 300 s, 400 s.

Finally, estimation of the wave flux which is given by Doyle et al [19]

$$F_{ms} = \rho \langle \delta v^2 \rangle \frac{\partial \omega}{\partial k}, \tag{25}$$

where $\partial\omega/\partial k$ represents the group velocity of the wave and the subscript stands for "magnetosonic". Bearing in mind the fact that the terms containing α are small compared with the other terms, we can derive the group velocity from Equation (19) by ignoring α terms, that is,

$$\frac{\partial \omega}{\partial k} = \frac{4c_s^2 V_A^2 k^3 - 2k\omega^2(V_A^2 - c_s^2)}{2\omega k^2 (V_A^2 - c_s^2) + 4\omega^3}. \tag{26}$$

Using typical values for a corona, i.e., $\langle \delta v^2 \rangle = 2 \times (43.9 \text{ km } s^{-1})^2$ [5], $c_s = 2.1 \times 10^7$ cm/s, $V_A = 2.5 \times 10^8$ cm/s, $\rho = 2.8 \times 10^{-15}$ g/cm^3 [10] and $2.0 \times 10^{-9} \leq k \leq 10^{-8}$ [23], the wave energy density F_{ms} turns out to be of the order of 10^6 erg cm^{-2} s^{-1} which is quite enough to replace the energy flux lost through optically thin emission and thermal conduction.

6. Results and Discussion

As pointed out, Equation (19) bears two solutions: one gives the dispersion relation of the fast mode, while the other gives the slow mode.

6.1. Slow Mode

Figure 1a shows damping length scale of the slow mode versus height from the coronal base. The damping length scale is the distance over which the original amplitude of the wave drops to its original amplitude times $1/e$. It is assumed that the slow mode wave is propagating in a plasma whose temperature is $T = 3 \times 10^6$ K and the magnetic scale height $\Lambda_B = 10^8$ m. We believe that the coronal plasma with these parameters are the most realistic one. In the figure, the shortest period wave lies at the bottom; the increase in the period ensues the increase in the damping length scale. As the period increases, the minimum of the graph becomes more prominent. Longer the period is, the more shifted to the right the minima becomes. The decrease in the damping length scale means that the wave mechanical energy is depleted faster in the corona around 250.000 km. The physics of the process may be outlined as below. A continuous spectrum of magnetosonic waves propagating along the open field lines may be generated by either granular motion of the plasma coming out of the convection region or magnetic reconnection or the migration of the footpoints of the loops. Generated short wavelength waves propagate along the weak lines and the long wavelength waves propagate along the strong lines [26]. This causes the phases of the waves on neighbouring field lines to become mixed in space. Priest [26] reports that if the above mentioned disturbances shake the field lines in phase at the footpoints, they become more and more out of phase as they propagate upwards. Steep gradients will be produced perpendicular to the field lines. This steep gradient combined with viscosity causes the waves to dissipate.

Table 1a. The variation of the damping length scale with height for Slow Mode with parameters $T = 3 \times 10^6$ K $\Lambda_p = 10^8$ m

p(s) / Z (m)	100	200	300	400
3,0E+06	3186	6345	9509	12676
5,0E+07	3208	6352	9511	12673
1,0E+08	3238	6354	9497	12646
1,5E+08	3247	6297	9389	12492
2,0E+08	3157	5969	8851	11752
2,5E+08	3329	5772	7997	10147
3,0E+08	3513	6295	8847	11105
3,5E+08	3594	6468	9237	11801
4,0E+08	3649	6532	9356	12008
4,5E+08	3692	6571	9415	12105
5,0E+08	3724	6599	9454	12164
5,5E+08	3746	6618	9479	12204
6,0E+08	3761	6630	9495	12228
6,5E+08	3769	6636	9503	12240
7,0E+08	3771	6638	9506	12244

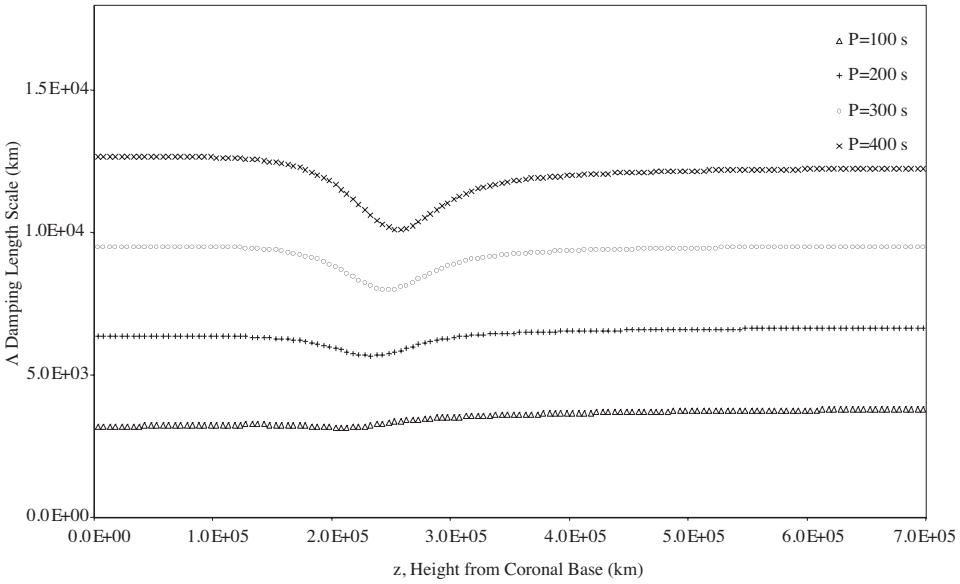

Figure 1a. The variation of the damping length scale with height for Slow Mode with parameters $T = 3 \times 10^6 K$ $\Lambda = 10^8$ m

Table 1b. The variation of the damping length scale with height for Slow Mode with parameters $T = 3 \times 10^6$ K $\Lambda_p = 10^7$ m

p(s) / Z (m)	100	200	300	400
3,0E+06	3183	6340	9502	12666
5,0E+07	3076	5458	7361	8957
1,0E+08	3201	5840	8063	9966
1,5E+08	3297	6077	8528	10676
2,0E+08	3382	6232	8836	11166
2,5E+08	3462	6342	9043	11504
3,0E+08	3534	6423	9187	11740
3,5E+08	3597	6486	9290	11906
4,0E+08	3650	6535	9363	12023
4,5E+08	3692	6572	9416	12107
5,0E+08	3724	6599	9454	12165
5,5E+08	3746	6618	9479	12204
6,0E+08	3761	6630	9495	12228
6,5E+08	3769	6636	9503	12240
7,0E+08	3771	6638	9506	12244

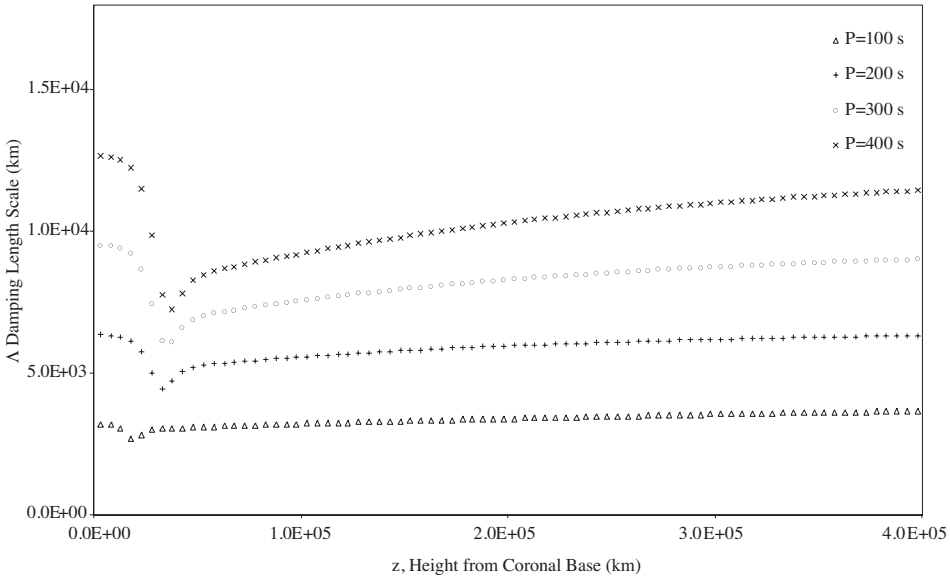

Figure 1b. The variation of the damping length scale with height for Slow Mode with parameters $T = 3 \times 10^6 K$ $\Lambda = 10^7$ m

In Figure 1b the period range is the same as in Figure 1a. But the minima are shifted towards the lower values of z and are deeper than that of Figure 1a. Above the coronal base the damping length scale shows a short drop to its minimum value and then rises mildly, more or less to its original value. Physically this means that after having lost its major portion of energy budget magnetosonic waves become more stable in the sense that their e-folding damping takes place over much greater lengths. To illustrate this physical reality we have drawn Figure 1d. In this figure there are three portions that are clearly different from one another. Region I illustrates e-folding damping with a constant damping length scale. In the region II is shown the wave amplitude with no damping. Region III shows again e-folding damping with a different length scale. If taken as a whole, this figure represents the behaviour of damping length scale with height. In summary, in a medium such as the solar corona where pressure and magnetic length scales are functions of height, damping length scale shows variation.

In Figure 1c with parameters $T = 1.3 \times 10^6$ K and $\Lambda_B = 10^9$ m. Damping length scale shows no variation. This means that the magnetosonic wave, no matter what the period is, will travel well defined distances before it experiences *e-folding* damping.

The results are given in Tables 1, 2 and in Figures 1, 2.

Table 1c. The variation of the damping length scale with height for Slow Mode with parameters $T = 1.3 \times 10^6$ K $\Lambda_p = 10^9$ m

p(s) / Z (m)	100	200	300	400
3,0E+06	3168	6335	9503	12671
5,0E+07	3169	6337	9505	12673
1,0E+08	3169	6337	9506	12674
1,5E+08	3170	6338	9506	12675
2,0E+08	3171	6339	9507	12675
2,5E+08	3173	6339	9507	12676
3,0E+08	3174	6340	9508	12676
3,5E+08	3175	6340	9508	12676
4,0E+08	3176	6341	9508	12676
4,5E+08	3176	6341	9508	12676
5,0E+08	3177	6341	9508	12676
5,5E+08	3177	6341	9509	12676
6,0E+08	3178	6341	9508	12676
6,5E+08	3178	6341	9508	12676
7,0E+08	3178	6341	9508	12676

6.2. Fast Mode

Figure 2a shows damping length scale of the fast mode versus height from the coronal base. It is assumed that the fast mode wave is propagating in a plasma whose temperature is $T = 3{\times}10^6$ K and the magnetic scale height $\Lambda_B = 10^7$ m. The behaviour of the damping

length scale is very peculiar. It starts with a certain value and gradually increases until the wave reaches 10000 km from coronal base. Then the damping length scale rises very steeply and reaches a value of 2.65×10^5 km. We may give an interpretation to this behaviour as follows: at around 10000 km from coronal base magnetosonic waves become extremely stable. In other words, if the physical parameters of the corona at the height of 10000 km were the same throughout the corona then those waves would survive and exit into the interplanetary medium. But after the waves passes through this relatively thin region they quickly become dissipational. The same behaviour is visible in Figure 2b. But this time it is assumed that the fast mode wave is propagating in a plasma whose temperature is $T = 3 \times 10^6$ K and the magnetic scale height $\Lambda_B = 10^8$ m. This change in parameters causes "the region of stability" shift to the height whose distance from the coronal base is 1.5×10^5 km. Physically speaking, in "the region of stability" phase mixing is less efficient than anywhere else. Above "the region of stability" phase velocity of the magnetosonic waves is probably becoming of the same order of magnitude of that associated with the ion cyclotron frequency. This brings about a condition of resonance wherein the mechanical energy of the waves is continuously and one-sidedly transferred to the ions of the medium. Indeed, magnetosonic waves are the MHD wave modes which appear in that part of the parameter space of the plasma pond neighbouring the ion cyclotron resonance bounding surface [28][29][30]. What we termed "the region of stability" appears at about 1.0×10^4 km in Figure 2a and at about 1.5×10^5 km in Figure 2b, respectively. These heights, we claim, are the ones where the phase velocity of the magnetosonic waves and the ion cyclotron frequencies become equal. In this resonance region the mechanical energy of the magnetosonic waves is sharply depleted and as a result the damping length scale drops.

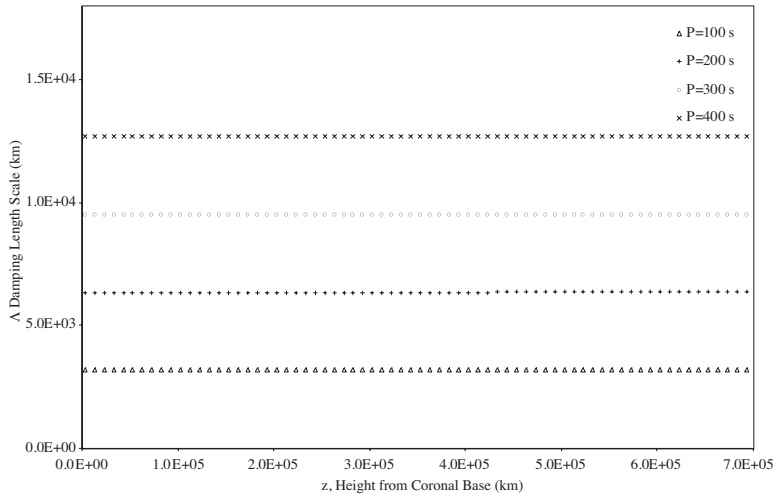

Figure 1c. The variation of the damping length scale with height for Slow Mode with parameters $T = 1.3 \times 10^6 K$ $\Lambda = 10^9$ m

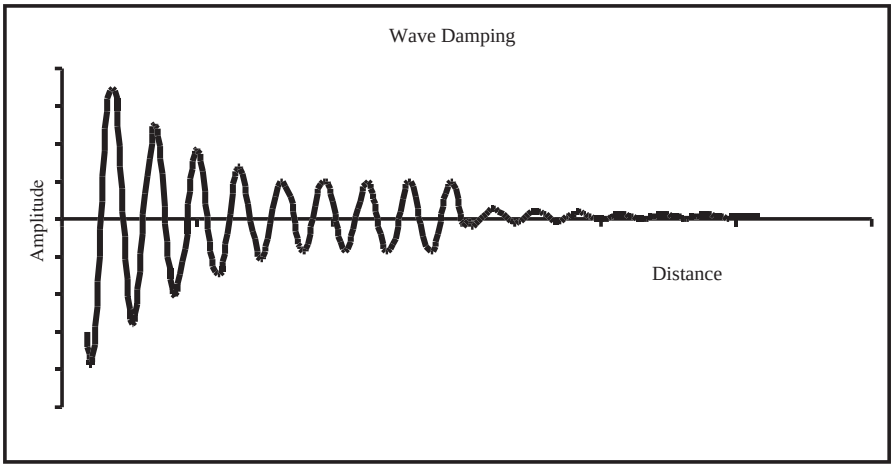

Figure 1d. Wave amplitude variation with distance. In this figure there are three portions that are clearly different from one another. On region I illustrated is e-folding damping with a constant damping length scale. In the region II shown is the wave amplitude with no damping; and finally on the region III again e-folding damping with a different length scale.

Table 2a. The variation of the damping length scale with height for Fast Mode with parameters $T = 3 \times 10^6$ K $\Lambda_p = 10^7$m

p(s) Z (m)	100	200	300	400
3,0E+06	177746	705442	1584932	2816216
5,0E+07	1709	2403	2938	3390
1,0E+08	2036	2855	3487	4022
1,5E+08	2330	3258	3976	4583
2,0E+08	2584	3605	4395	5065
2,5E+08	2799	3897	4747	5468
3,0E+08	2976	4136	5036	5798
3,5E+08	3117	4328	5266	6062
4,0E+08	3228	4478	5446	6267
4,5E+08	3312	4592	5583	6424
5,0E+08	3373	4676	5683	6538
5,5E+08	3416	4734	5753	6617
6,0E+08	3443	4771	5797	6668
6,5E+08	3457	4790	5820	6694
7,0E+08	3461	4796	5826	6701

Table 2b. The variation of the damping length scale with height for Fast Mode with parameters $T = 3 \times 10^6 K$ $\Lambda_p = 10^8$ m

p(s) / Z (m)	100	200	300	400
3,0E+06	166898	662637	1488867	2645586
5,0E+07	118146	464234	1041036	1848555
1,0E+08	108582	416865	930661	1649974
1,5E+08	1697822	3271486	6659935	11450477
2,0E+08	11351	40203	88199	155380
2,5E+08	3370	5931	9292	13665
3,0E+08	3046	4339	5423	6420
3,5E+08	3128	4357	5319	6142
4,0E+08	3229	4483	5454	6279
4,5E+08	3312	4593	5584	6425
5,0E+08	3373	4676	5683	6538
5,5E+08	3416	4734	5753	6617
6,0E+08	3443	4771	5797	6668
6,5E+08	3457	4790	5820	6694
7,0E+08	3461	4796	5826	6701

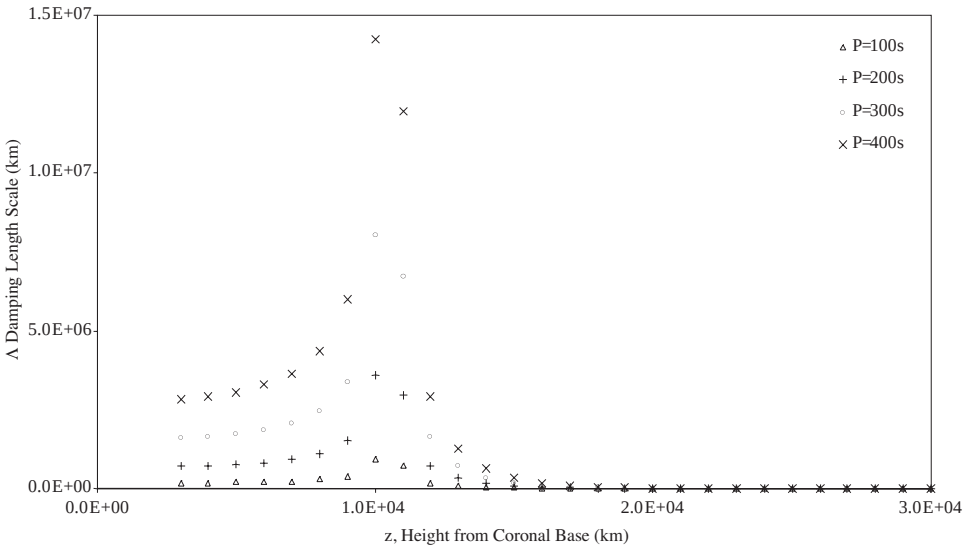

Figure 2a. The variation of the damping length scale with height for Fast Mode with parameters $T = 3 \times 10^6 K$ $\Lambda = 10^7$ m

Table 2c. The variation of the damping lenght scale with height for Fast Mode with parameters $T = 1.3 \times 10^6$ K $\Lambda_p = 10^9$ m

p(s) Z (m)	100	200	300	400
3,0E+06	1,33E+06	5,33E+06	1,20E+07	2,13E+07
5,0E+07	8,64E+05	3,46E+06	7,78E+06	1,38E+07
1,0E+08	6,12E+05	2,45E+06	5,50E+06	9,78E+06
1,5E+08	4,71E+05	1,88E+06	4,24E+06	7,53E+06
2,0E+08	3,86E+05	1,54E+06	3,47E+06	6,17E+06
2,5E+08	3,32E+05	1,33E+06	2,98E+06	5,30E+06
3,0E+08	2,96E+05	1,18E+06	2,66E+06	4,72E+06
3,5E+08	2,71E+05	1,08E+06	2,44E+06	4,33E+06
4,0E+08	2,54E+05	1,01E+06	2,28E+06	4,06E+06
4,5E+08	2,43E+05	9,68E+05	2,18E+06	3,87E+06
5,0E+08	2,35E+05	9,36E+05	2,10E+06	3,74E+06
5,5E+08	2,30E+05	9,15E+05	2,06E+06	3,66E+06
6,0E+08	2,27E+05	9,03E+05	2,03E+06	3,61E+06
6,5E+08	2,25E+05	8,98E+05	2,02E+06	3,59E+06
7,0E+08	2,26E+05	8,99E+05	2,02E+06	3,59E+06

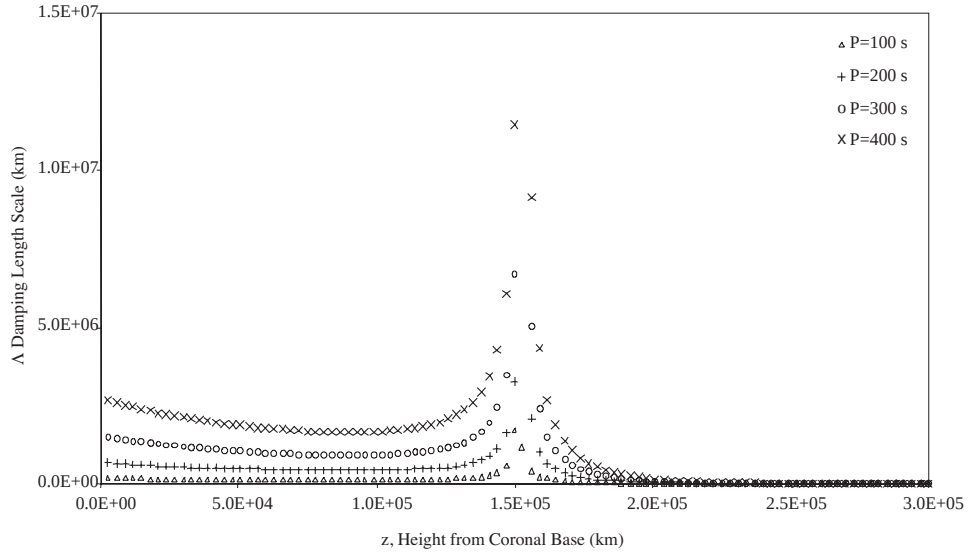

Figure 2b. The variation of the damping length scale with height for Fast Mode with parameters $T = 3.0 \times 10^6 K$ $\Lambda = 10^8$ m

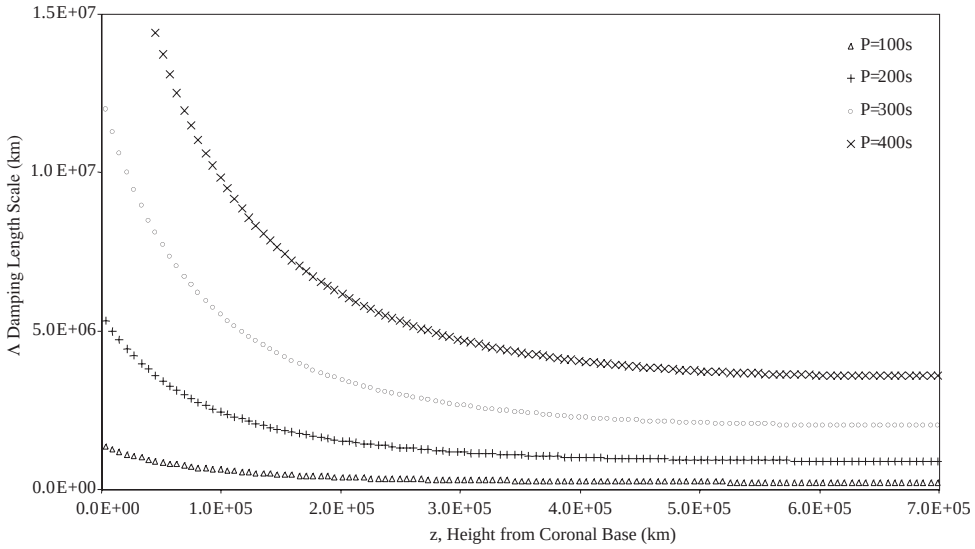

Figure 2c. The variation of the damping length scale with height for Fast Mode with parameters $T = 1.3 \times 10^6 K$ $\Lambda = 10^9$ m

What we have speculated in the above paragraph about the physical cause of the drop of the damping length scale can be checked by analysing the same problem in the context of Maxwell-Boltzmann equation. In this approximation, the relation between the ion cyclotron frequency and the phase velocity of the magnetosonic waves appears self-consistently in the dispersion relation. We shall set ourselves to this task in a future study.

7. Conclusion

Our investigation of the wave propagation characteristics of the magnetosonic waves in the solar corona yields such results as to make us propose that these waves carry enough energy flux to heat the corona. If the nonthermal broadening of the coronal lines are as strong as Doyle et al [4][19] claim to be, then the wave mechanical flux density turns out to be of the order of 10^6 erg cm^{-2} s^{-1}. This is high enough to replace the energy lost via optically thin emission and the thermal conduction down to the transition region. This is, of course, not to claim that the wave dissipation is the sole process to heating the solar corona. Surely, there are other agents such as magnetic reconnection, current dissipation and so on at work with different efficiencies at different regions of the solar corona. All we wish to draw attention to is the potentiality of the magnetosonic waves as a heat source. Although we have shown that the magnetosonic waves are dissipational and they carry enough flux to replace that lost, we could not quantitatively touch upon the physical process with which the heat transfer is realized. In a qualitative discussion,

we remind the reader that the ion cyclotron resonance and/or phase mixing are two likely candidates among many other. This problem can be solved in kinetic approximation, i.e., by the solution of Vlasov equation.

References

[1] Longair, M.S., 1992, *High Energy Astrophysics,* Vol. 1, pp. 358, CUP, Cambridge.

[2] Tappin, S.J., Simnett, G.M., Lyons, M.A., 1999, *Astron. Astrophys.,* **350**, 302.

[3] McKenzie, J.F., Banaszkiewicz, M., Axford, W.I., 1995 *Astron. Astrophys.,* **303**, L45.

[4] Doyle, J.G., Teriaca, L., Banerjee, D., 1999, *Astron. Astrophys.,* **349**, 956.

[5] Banerjee, D. et al., 1998, *Astron. Astrophys.,* **339**, 208.

[6] Saba, J.L.R. & Strong, K.T., 1991, *The Astrophysical Journal,* **375**, 789.

[7] Hassler, D.M. et al., 1990, *The Astrophysical Journal,* **348**, L77.

[8] Braginskii, S.I., 1965, *Transport processes in plasma, in Rev. of Plasma Physics,* ed. M.A. Leontovich, Vol I, pp. 205, Consultants Bureau, NY.

[9] Ulmschneider, P., 1996, *private communication.*

[10] Priest, E.R., 1984, *Solar Magnetohydrodynamics,* D.Reidel Pub. Co., Dordrecht.

[11] Ruderman, M.S. et al., 1996, *Journal of Plasma Physics,* Vol. 56, part 2, pp. 285.

[12] Melrose, D.B., 1989, *Instabilities in Space and Laboratory Plasma,* CUP, Cambridge.

[13] Hollweg, J.V., 1973, *The Astrophysical Journal* , **181**, 547.

[14] Doschek, G.A. et al., 1976, *The Astrophysical Journal Suppl.*, **31**, 417.

[15] Feldman, U. et al., 1976, *The Astrophysical Journal Suppl.*, **31**, 445.

[16] Mariska, J.T., Feldman, U. & Doschek, G.A., 1979, *The Astrophysical Journal*, **73**, 361.

[17] Shine, R.A., 1976, *The Astrophysical Journal Lett.* , **210**, L 107.

[18] Roussel-Dupre, R., Francis, M.H., & Billings, D.E., 1977, in *Proc. OSO-8 Workshop,* Univ. of Colorado, Boulder.

[19] Doyle, J.G., Banerjee, D., and Perez, M.E., 1998, *private communication.*

[20] Ruderman, M.S., 1991, *Solar Physics,* **131**, 11.

[21] Van der Linden, R.A.M. & Goosens, M., 1991, *Solar Physics,* **131**, 79.

[22] Cargill, P.J., & Hood, A.W., *Solar Physics,* **124**, 101.

[23] Porter, L.J., Klimchuk, J.A., & Sturrock, P.A., 1994a, *The Astrophysical Journal,* **435**, pp. 482.

[24] Porter, L.J., Klimchuk, J.A., & Sturrock, P.A., 1994b, *The Astrophysical Journal,* **435**, pp. 502.

[25] Oliver, R., Murawski, K. and Ballester, J.L. 1998 *Astron. Astrophys.,* **330**, 726

[26] Priest, E.R., 1994 in *Plasma Astrophysics*, Benz, A.O. and Courvoisier, T.J.-L. (eds). Springer-Verlag, Berlin.

[27] Oliver, R., Ballester, J.L., Hood, A.W., and Priest, E. R. 1993 *Astron. Astrophys.,* **273**, 647

[28] Nishikawa, K. and Wakatani, M., 1994, *Plasma Physics,* Springer Verlag, Berlin.

[29] Shohet, J.L., 1971, *The Plasma State*, Academic Press, Inc., NY.

[30] Boyd, T.J.M. and Sanderson, J.J, 1969, *Plasma Dynamics,* Thomas Nelson and Sons LTD.,London